Quantum Efficiency Calibration of HRC-I

Almus Kenter

1 HRC-I Quantum Efficiency

1.1 Introduction

The Quantum Efficiency of the HRC-I was determined as a function of energy and position by combining data from three distinct data sets: These data sets were: XRCF HRC-I on axis Effective Area (EA) measurements, SAO HRC-I Flat Field (FF) illumination tests and Synchrotron data measurements of non-flight coated MCP detectors.

The XRCF EA measurements were obtained with the flight instrument in the converging beam of the High Resolution Mirror Assembly (HRMA). Although the XRCF measurements were made with the flight instrument, the instrument was not in final flight configuration. Hardware modifications to the HRC instruments were implemented after the XRCF calibration to correct several hardware problems. These problems caused lower than expected QE values and large spatial non-uniformities particularly in the HRC-S detector; the HRC-I detector was relatively unaffected. The nature of the HRC problems and ensuing modifications are discussed in detail elsewhere (Murray, S. *et al.,* 1997).

The SAO flat field illumination tests were performed on the HRC-I detector in its final flight configuration. These flat field tests measured the QE of the HRC-I detector with X-rays at $\approx$ normal incidence to the MCP surface. A wholly seperate series of measurements were made later to measure the effect of incidence angle on relative QE. These angle-of-incidence measurements were later used to model and take into account the effect of the finite angle converging beam of the HRMA on MCP QE.

The Synchrotron data was obtained at the Daresbury Synchrotron using non-flight, HRC-S type (Philips MCPs) in non-flight like detectors, with non-flight like electronics. These "representative" detectors were coated with CsI at the University of Leicester. In contrast the HRC-I flight MCPs were manufatuctured by the Galileo Electro Optics Corporation (GEOC) and were coated with CsI at SAO. The synchrotron data measured the QE of the MCP detectors near the Cs and I M edges and between 277 and 350 eV. No cross calibration of these representative MCPs were done with the HRC-I detector. Due to the different heritage and the lack of cross-calibration, there may be large systematic errors introduced by incorporating this data into the HRC-I instrument calibration. The synchrotron data were also obtained at "normal incidence".

The QE of the HRC-I instrument is determined by the product of the Ultra-Violet Ion Shield (UVIS) transmission and the HRC-I MCP QE. The uniformity and the transmission of the UVIS has been measured extensively at SAO and at the Bessy Symchrotron and are known with little relative uncertainty. The measurements of the HRC-I UVIS are discussed elsewhere within this calibration report.

The method for determining the QE of the HRC-I detector is to first determine the QE of the CsI coated MCPs without the UVIS at a set number of energies for normal incidence illumination; this entails dividing out the transmission of the UVIS and dividing out the HRMA effective area from the HRC-I/HRMA EA measurements. These discrete MCP QE values are combined with an interpolation scheme to determine the QE versus energy for the CsI coated MCPs on a finer energy scale. The synchrotron QE data near the Cs and I M edges is then scaled appropriately and spliced into MCP QE versus energy data. The QE of the overall HRC-I detector is then obtained by multiplying the MCP QE by the HRC-I UVIS transmission. The appropriate correction for the HRMA cone angles are then applied.

This section of the HRC calibration report will present : the spatially averaged QE of the HRC-I detector as a function of energy, the QE versus position of the HRC-I detectors (spatial uniformity) and the EA of the HRC-I/HRMA combination as a function of energy. Furthermore the limited energy energy resolution of the HRC-I and the overall uncertainty of these data products will be discussed.

Due to the lack of consistent data below 277 eV, no QE or EA data products will be presented for $E < 250$ eV for the HRC-I detector. A series of laboratory measurements are presently being planned to fill in this gap in the HRC-I calibration, furthermore this energy range will be investigated during the on-orbit calibration.

2 XRCF and Flat Field Measurements

2.1 XRCF Effective Area Measurements

The Effective Area (EA) of the HRMA/HRC-I was measured at the XRCF. Details of these measurements and of the XRCF calibration facility are discussed elsewhere (D.Patnaude *et al.,* 1998 ,J.Kolodziejczak *et al.,* 1995).

Using these XRCF determined EA measurements, MCP QE values were determined by dividing out the XRCF appropriate HRMA effective mirror area and the transmission of the UVIS. Only on-axis EA measurements were used.

In addition to the HRMA effective area, the effects of the HRMA cone angles on MCP QE values had to be taken into account. A detailed discussion of the experimental campaign to determine the effect of HRMA cone angles on QE is an appendix to this calibration report. The HRMA cone angle correction for the HRC-I is presented in Figure 7 which shows that it differs significantly from 1.0 (normal incidence) only for energies $<$ 500 eV for the HRC-I.

The X-ray sources used at XRCF were an Electron Impact Source (EIPS) with various anodes and filters; a Rotating Anode Source (RAS) with either a High Resolution Erect Field Spectrometer (HIREFS) (used as a monochromator) or a Double Crystal Monochromator (DCM).

The HIREFS source was intended to provide EA measurements for energies from 400 to 2000 eV. In practice, the HIREFS data suffered from large spatial non-uniformities over the input face of the HRMA. Furthermore, the HIREFS suffered from higher-order spectral contamination of the continuum source and from strong spectral contamination by Tungsten M lines near 1.7 keV. The poor spectral quality of the HIREFS data and the low energy resolution of the HRC-I detector necessitated a complex "boot-strapping" process to extract HRC-I/HRMA EA values. The ensuing large systematic errors made the HIREFS data useful only for qualitative comparison with other data. HIREFS determined QE data were not used to determine the HRC-I QE.

The DCM data comprises the largest and best XRCF data set; it had little higher order contamination and the X-ray beam was relatively uniform over the face of the HRMA. The DCM data,however, was limited to $E > \sim 2$ keV. All DCM measurements were incorporated into the QE model except two points at 8 keV and at 9 keV; these two high energy points were high and indicated that the QE of the HRC-I was actually increasing rapidly with energy above 7 keV. The values and the trend are not expected from either the photocathode or the MCP glass and in fact, synchrotron data with CsI coated MCPs indicate that the QE is decreasing from 6 through 9 keV. These two DCM data points were eliminated from the input data set and the QE was then extrapolated out to 10 keV from the 6.3 keV eV and 7 keV DCM measurements.

Only one EIPS EA measurement at 277 eV was used for the HRC-I QE calibration. Other measurements at 183 eV were not consistent and have been left out.

The HRMA cone angle correction differed significantly from 1.0 only for the 277 eV XRCF data point. Applying the cone angle correction to the XRCF determined QE measurement, gave a value identical (within the uncertainties) to the flat field QE value.

Even though the XRCF data were collected with the flight instrument, the instrument was not in final flight configuration. The HRC instrument, as first built, had some hardware problems that only became manifest during the XRCF calibration program. In essence, a high amplitude 91kHz ripple on the High Voltage power supply made it necessary to operate the detectors with high unflight-like thresholds. These settings affected the low energy response of the HRC instruments.

2.2 SAO Flat Field QE and Uniformity Measurements

Following the XRCF calibration the HRC instrument returned to SAO for modification and flat-field illumination tests. The problems with the 91kHz HV power supply ripple were fixed. HV settings and detector threshold levels were then optimized. Flat field illuminations were performed at three energies prior to implementing any changes and at eight energies after completing all the fixes and after establishing new flight thresholds. The purpose of the Flat Field illuminations were to determine the average and spatially dependent QE of the HRC-I detector.

During Flat Field testing, the HRC instrument was mounted to an $\sim$ 7 meter X-ray pipe to provide approximately normal incidence X-ray illumination. A series of adapter flanges were used to mount the instrument externaly to the vacuum chamber and to illuminate the HRC-I and each of the HRC-S segments separately. This mounting scheme allowed access to the HRC electronics for testing and modification during operation. Initial flat field illuminations of the HRC-I detector were performed with a flange that illuminated the center HRC-S segment simultaneously at the expense of uniform illumination of the HRC-I. These initial HRC-I flat field illuminations were the only ones performed at the pre-fix, XRCF settings. These "pre-fix" HRC-I flat field illuminations suffer from gross beam non-uniformity and are not useful for determining the uniformity of the HRC-I detector. The "post-fix" flat fields were performed with a new flange and with uniform HRC-I illumination.

X-ray illumination was provided by a Manson Model 5 multi-anode electron impact source. The anodes and filter combinations listed in Table 1 were used. The SAO Flat Field facility is depicted in Figure 1.

Line	Energy	Filter	MFPs	V_A	L/C
B Kα	183 eV	7 μ parylene-C	5.87	600 V	48.4
C Kα	277 eV	33 μ polypropylene	5.94	1000 V	171
O Kα	525 eV	2 μ Cr	4.67	1000 V	29.3
Ni Lα	851 eV	2 μ Cu	3.80	2500 V	2.55
Al Kα	1487 eV	50 μ Al	5.40	4000 V	38.9
Ag Kα	2984 eV	10 μ Ag	4.86	6000 V	0.60
Ti Kα	4511 eV	150 μ Ti	6.80	10000 V	6.73
Fe Kα	6404 eV	125 μ Fe	6.97	10000 V	1.78

Table 1: Summary of line energies, filters, thicknesses, anode voltages, and predicted line-to-continuum ratio of the X-ray source for HRC-I flat fields.

The absolute beam intensity at the input of the HRC was measured using a Manson Model 04 flow proportional counter which was mounted on a retractable arm. This Beam Normalization Detector (BND) was not operated concurrently with the HRC as it had a slow gas leak through its window which spoiled the vacuum too

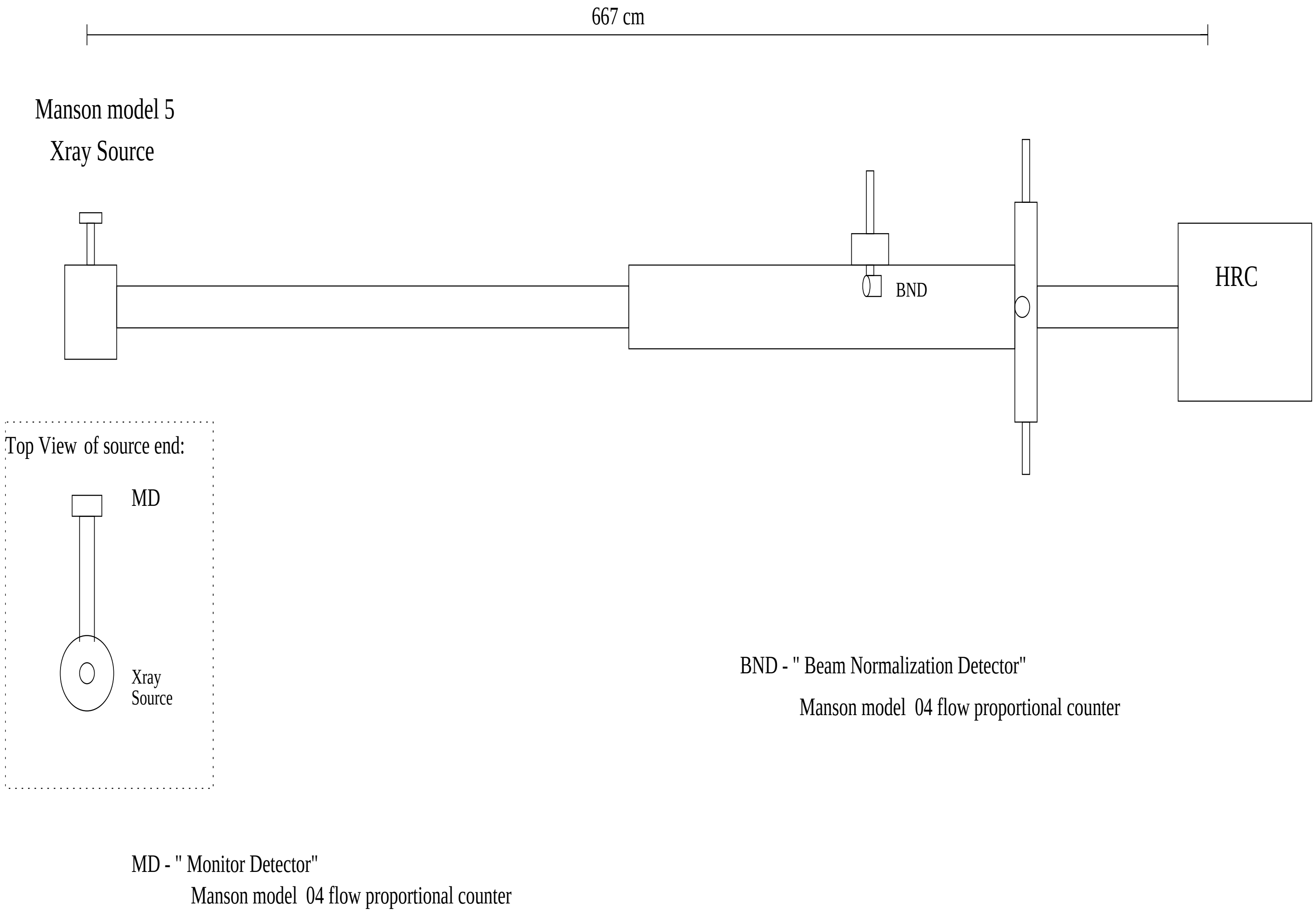

Figure 1: Facilities at the SAO HRC laboratory used for flat-field illumination of the HRC detectors.

close to the input face of the MCPs. Absolute flux measurements and temporal monitoring were performed by first cross calibrating a second Manson model 04 Monitor Detector (MD) flow proportional to the BND. This MD was close to the actual X-ray source and operated concurrently with the HRC detectors. By using the MD rates and the MD to BND cross-calibration the QE of the HRC detector was measured. The QE of the HRC was calculated as:

$$QE_{hrc} = \frac{R_{hrc}}{I_{hrc}\Omega_{hrc}} \tag{1}$$

Where:

$$I_{hrc} = \frac{R_{MD}}{QE_{BND}\Omega_{BND}} \times (\frac{BND}{MD})_{cc} \tag{2}$$

and $(\frac{BND}{MD})_{cc}$ is the BND to MD cross calibration ratio. The QE of the proportional counters were calculated from their window properties and mechanical dimensions; no cross calibration to any standards were performed. The window transmission of the BND and MD proportional counters were measured extensively using a McPherson Monochromator and subsequently modeled at SAO. The effective counter depth provided by the manufacturer was used. Gas pressure, composition (CH_4 or $P10$) and temperature were controlled and/or measured throughout the tests.

The HRC-I was illuminated for a set time to insure that at least 10^7 events were collected for all the anodes excepting Boron, where only $\sim 3 \times 10^6$ events were collected.

During the Flat Field illumination tests of the HRC detectors, the electronics were modified so as to allow a data rate $\approx 10\times$ the telemetry limit of $\approx 188\ sec^{-1}$. In practice, data rates were intentionally limited to $1200 - 1400\ sec^{-1}$ for the HRC-I for all energies except for Boron. The Boron data were flux limited. The $\times 10$ operation of the HRC necessitated that dead-time corrections be calculated and applied to the flat field QE values.

The dead time for the HRC detectors has been independently measured to be $\tau = 68.5\mu$-seconds; the majority of this is due to an ADC conversion time. Dead time corrections can be applied to the Flat-Field HRC QE values by considering the instrument as a non-paralyzable (non-extendable dead time) detector with a characteristic dead time of $\tau = 68.5\mu$-seconds. Using just the measured rates of $R_{meas} \sim 1200\ sec^{-1}$, without correction would cause an underestimate of the true QE, by $\sim 9\%$.

It can be easily shown under the above assumptions that:

$$\frac{QE_{true}}{QE_{meas}} = \frac{R_{true}}{R_{meas}} = \frac{1}{1 - R_{meas}\tau} \tag{3}$$

Where the true QE values are the "zero-rate" limits.

The QE values as quoted are averaged over the entire photocathode coated HRC-I MCP area. The line to continuum ratios as listed in Table 2 are based on theoretical modeling of the bremstrahlung and line emission as modified by the X-ray filter. Several of the flat field QE points were suspect when compared with QE measurements from XRCF data. The Ag L_α line, which had a very low L:C ratio and an anomolously low QE measurement, was rejected from further consideration. The Ti K value as quoted is actually a mixture of the the K_α and K_β lines where the normal K_β:K_α ratio is increased by the effect of the $125\mu m$ Ti filter ($\times \sim 1.5$). The enhanced ratio and the fact that the two Ti lines straddle a significant photocathode edge (I L_{III} edge at 4550ev) caused a significant overestimate of the Flat Field QE HRC at 4510 eV. This FF QE measurement was excluded from the calibration.

The Fe anode-Fe filter combination also enhanced the K_β:K_α ratio however it did not fall near any detector feature. The QE at Fe K as determined from the flat field illumination was $\sim 5\%$ lower than XRCF data in the same energy region. No systematic errors could account for this discrepency. The Fe flat field point was also left out as input to the QE model. The high K_β:K_α ratios for the Ti and Fe anodes were confirmed using an X-ray CCD camera; this CCD data is presented in the HRC-S section of this report.

HRC-I QE		
Element	Energy (eV)	QE
B	183	0.062
C	277	0.20
O	525	0.12
Ni	851	0.27
Al	1487	0.31
Ag	2980	0.093
Ti	4511	0.10
Fe	6404	0.14

Table 2: Table of Flat Field (normal incidence) HRC-I QE values (with UVIS) corrected for dead time. Values are averaged over the CsI coated region of the HRC-I detector.

2.3 Uniformity Data

The Flat Field illumination tests, in addition to providing QE measurements allowed us to examine the uniformity of the HRC-I detector response. The HRC-I flat fields exposures were used to create FITS format QE maps and surface plots normalized to the average QE of the detector. The two of the eight surface plots are are presented in Figures 2 and 3. The FITS QE maps for all measured energies are available on the HRC calibration webpage.

2.4 Energy Resolution

The inherent energy resolution of the HRC-I detector was investigated by examining the effect of incident X-ray energy on detected pulse height. The detected pulse height of the HRC-I versus incident energy is presented in Figure 4. It is evident that the HRC-I has some limited energy resolution for an ensemble of photons, particularly at energies < 1keV. This energy versus pulse-height data were taken as part of the flat field uniformity tests and is for normal incidence radiation. The effect of the finite HRMA cone angles on the energy versus pulse-height has been investigated for CsI coated HRC-I flight type MCPs. No significant difference between pulse height distributions from normal incident X-rays and from X-rays averaged over the incident angles from the HRMA mirror was noted.

The dependance of HRC-I pulse height on incident X-ray energy was further quantified by fitting the background-subtracted pulse height distribution to the sum of two Gaussian distributions. The functional form of the two-Gaussian distribution product was:

$$P = \frac{N_1}{\sqrt{2\pi\sigma_1}} e^{\frac{(c_i - C_1)^2)}{2\sigma_1^2}} + \frac{N_2}{\sqrt{2\pi\sigma_2}} e^{\frac{(c_i - C_2)^2)}{2\sigma_2^2}} \quad (4)$$

The parameters, N_1 C_1 σ_1 and N_2 C_2 σ_2 as a function of the measured energies are presented in Table 3. It can be noted from the parameters that N_1 plus N_2 don't always add up to unity; this is because there are events in the saturated pulse height channel which have been excuded from the fitting process.

3 Synchrotron Measurements

A series of measurements were performed on CsI coated MCPs at the Daresbury synchrotron. The purpose of these measurement was to measure the absolute and relative QE of MCPs over the AXAF energy band. Special

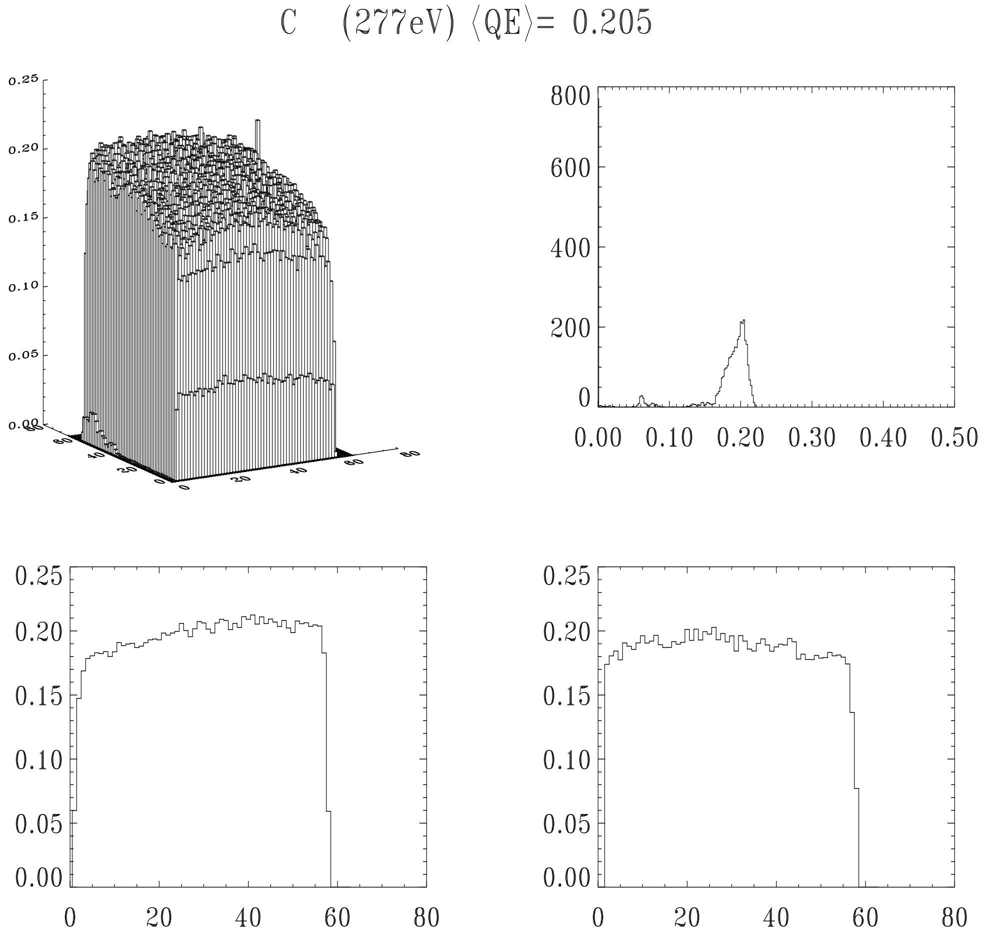

Figure 2: Surface plot of flat field normalized to average QE. $\sim 10 \times 10^6$ detected events. Surface plot is HRC-I rebinned into 64 $\times$ 64 pixels; each pixel then corresponds to an HRC coarse position of 1.646 mm which is $\approx$ 0.5 arc-sec. Distribution of QE in each square coarse position pixel and central slices in "U" and "V" axes are shown.

Energy	N_1	C_1	σ_1	N_2	C_2	σ_2
183 eV	0.70	63.48	21.3	0.23	102.09	27.7
277 eV	0.91	67.5	23.5	0.08	107.53	37.3
525 eV	0.83	85.07	27.5	0.15	133.24	40.4
851 eV	0.77	95.70	29.4	0.20	148.7	43.8
1487 eV	0.68	95.91	30.9	0.29	152.38	46.6
2984 eV	0.56	90.92	30.5	0.39	155.59	49.9
4511 eV	0.57	89.44	30.0	0.37	157.72	49.3
6404 eV	0.50	90.86	31.3	0.41	164.86	50.7

Table 3: Parameters of HRC-I pulse height as sum of two Gaussian versus X-ray illumination energy.

emphasis was placed on sampling near the various detector features such as the absorbtion edges of Cs and I. The CsI photocathode coatings were applied at the University of Leicester to Philips (HRC-S) type MCPs

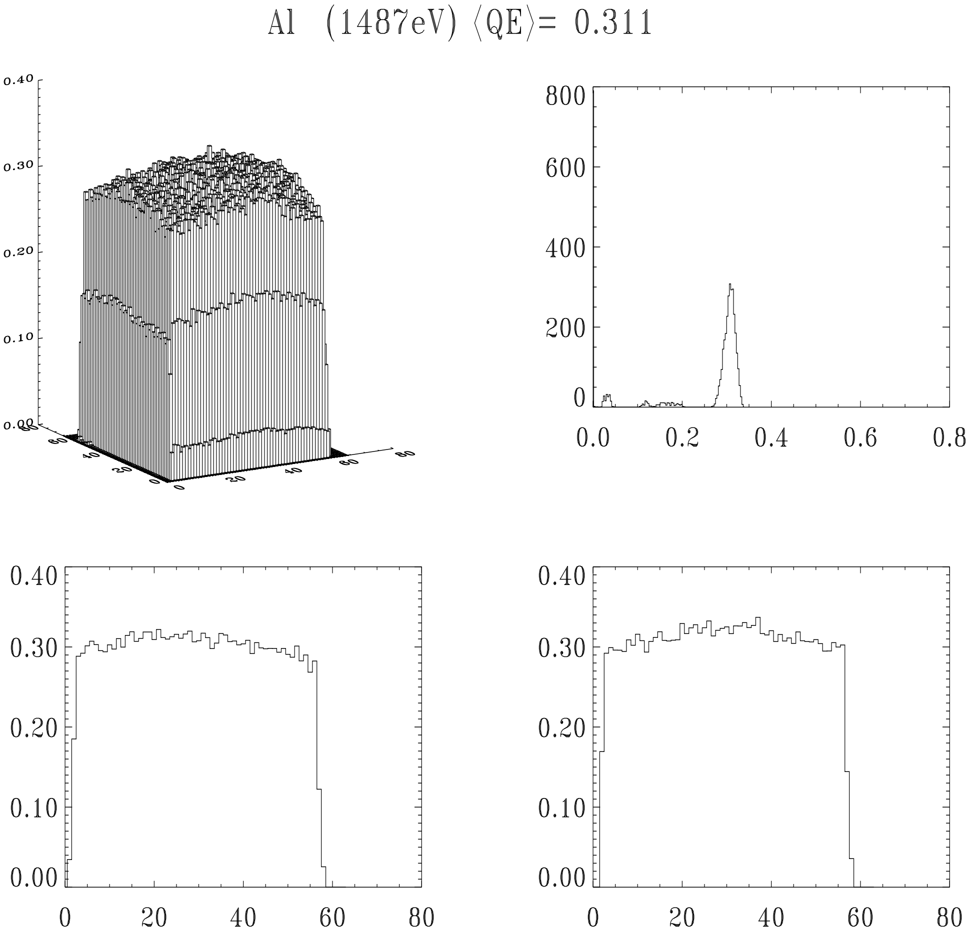

Figure 3: Surface plot of flat field normalized to average QE. $\sim 10 \times 10^6$ detected events. Surface plot is HRC-I rebinned into 64 $\times$ 64 pixels; each pixel then corresponds to an HRC coarse position of 1.646 mm which is $\approx$ 0.5 arc-sec. Distribution of QE in each square coarse position pixel and central slices in "U" and "V" axes are shown.

wheras the actual HRC coatings were applied at SAO. The representative MCPs were then incorporated into detectors and tested at the Daresbury synchrotron which was operated in low current mode to allow operation of the detectors in single photon counting mode. The various Daresbury calibration campaign are discussed in detail elsewhere (R.Rideout *et al* 1998, S.Pierce 1996).

Two subsets of the synchrotron data were incorporated as input to the HRC QE calibration. The first set of data was collected in January 1995 at beam line 6.1 of the Daresbury Synchrotron. This data spanned the energy band of 50-350eV in 1eV steps using a 1200 line-per-mm Miyake plane grating monochromator. The spectrum of the monochromator and associated optics had been measured previously using a Tungsten grid reference detector. High rates in the MCP detector necessitated that the data be corrected for dead time and gain suppression. Following the synchrotron measurements, the relative QE versus energy data were normalized to a laboratory measurement of QE at Carbon K (277eV) at the University of Leicester. This data was then again normalized to the Flat Field QE value at 277eV.

The second set of Daresbury Synchrotron data was collected in October 1997 on beamline 1.1. This data spanned the energy band of $\sim$ 450 to 800eV in 0.5 eV steps using a Ni(3) grating and used a flow proportional counter for absolute normalization of the beam. Unfortunately, the input flux was spoiled by suspected Carbon

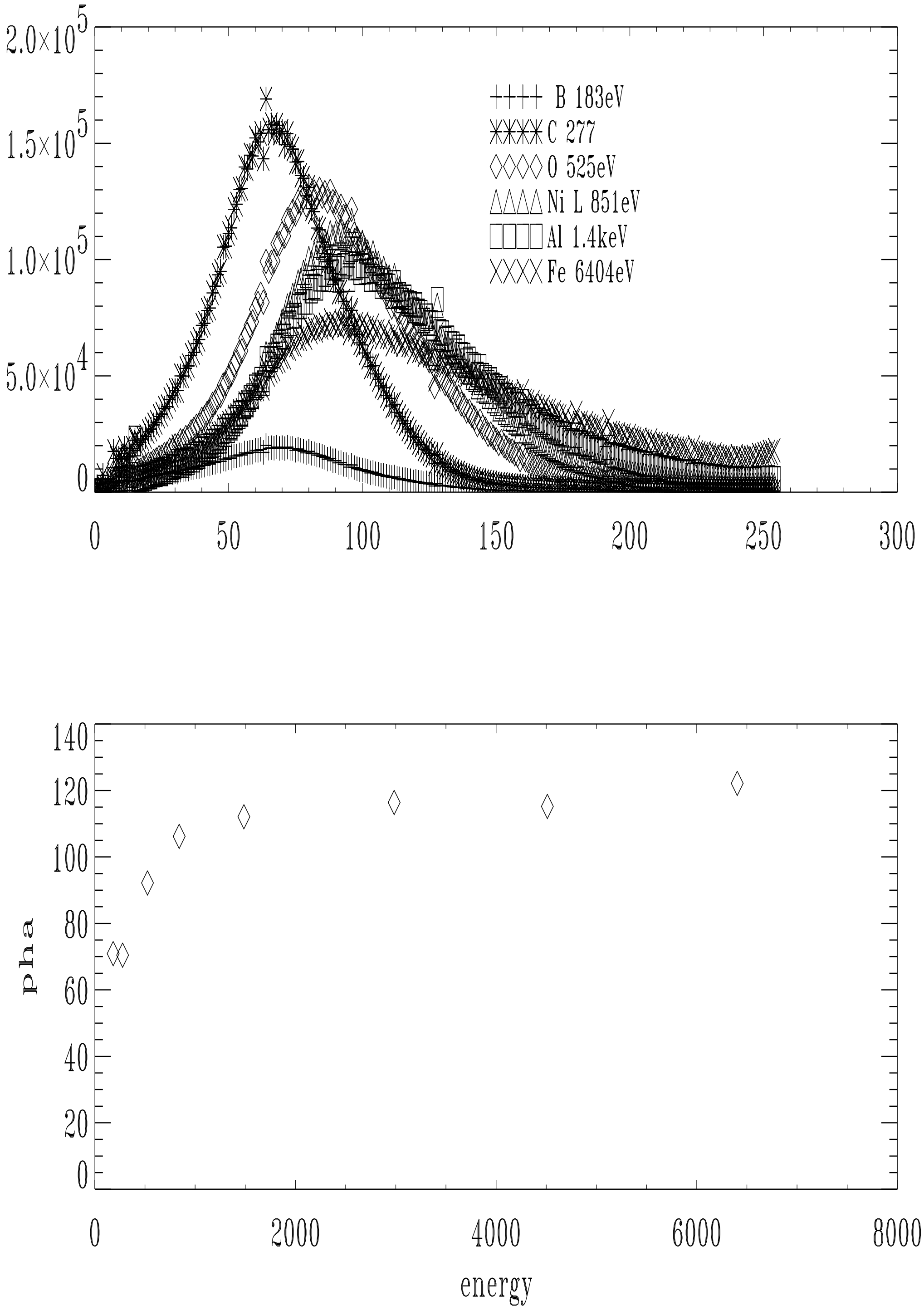

Figure 4: Pulse height distributions versus energy and centroids of pulse height versus energy for the HRC-I detector. It is evident that the HRC-I has some limited inherent energy resolution.

contamination of the beamline optics and higer order Carbon and Oxygen spectral contamination. Details of this second data set are discussed in detail by Rideout *et al., 1998.*

3.1 MCP QE model- interpolation to a finer energy scale

The QE of the CsI coated HRC-I MCPs was interpolated to a finer energy grid using: three sets of input points. These input points were: the flat field QE measurements, QE values obtained from XRCF EA measurements and the synchrotron data from 277 through 350 eV.

The interpolation scheme is outlined in a memo by M. Juda (1997) and is based on earlier photocathode work of Henke, Knauer and Premaratne (1981). The model will now be presented in brief.

The QE of CsI coated MCPs can be written as

$$QE_{MCP} = f(1 - e^{y(E)}) \tag{5}$$

Where $f = 0.58$ is the open area ratio of the MCPs and represents the maximum possible QE. $y(E)$ is the mean photo-electron yield of the photocathode as a function of energy. The QE is then the Poisson probability of producing a photo electron yield of one or greater given a mean yield of $y(E)$.

The yield, $y(E)$, written as

$$y(E) = \Lambda(E)\rho_{CsI}\mu(E)_{CsI} \tag{6}$$

is just the photo absorbtion within an electron range of the photocathode surface, where $\Lambda(E)$ is the electron range, $\mu(E)_{CsI}$ is the mass absorbtion coefficient of CsI and ρ_{CsI} is the mass density of CsI. The function $\Lambda(E)$ contains all the complex physics of electron transport of the photocathode. Furthermore, $\Lambda(E)$ is reported to vary weakly as a function of energy (Henke, Knauer and Premaratne 1981).

From the above two equations one can solve explicitly for $\Lambda(E)$ as a function of the discretely measured MCP QE values QE_i.

$$\Lambda(E_i) = \frac{ln(1 - \frac{QE_i}{f_{pore}})}{\mu(E)_i)\rho} \tag{7}$$

A spline interpolation was performed between the $\Lambda(E_i)$ points. The resulting MCP QE model was then determined by incorporating the $\Lambda(E)$ interpolation into Equations 6 and 5.

The resulting MCP QE "model" depends on the (1993) Henke Cs and I mass absorbtion coefficients to determine jump ratios and photocathode edge locations. Comparing the interpolated MCP QE with synchrotron data showed that the interpolated jump ratios are too high and true edge locations are displaced to higher energies. This displacement of M edges of high Z materials has been observed elsehwere (Owens *et al., 1996.*

The second set of synchrotron data that spanned the Cs and I M edges was rescaled to match the flat field QE value at 525 eV by the use of an additive constant. This synchrotron data was then used to "replace" the interpolated data between 600 and 800 eV. The use of an additive constant was justified on account of the suspected higher order contamination.

A list of XRCF and FF MCP QE values with associated error values that were input to the interpolation scheme is presented in Table 3.1.

The overall interpolated QE of the HRC-I MCPs is presented in Figure 5. The QE of the HRC-I CsI coated MCPs is presented in Figure 6 in conjunction with the XRCF HIREFS data that were **not** used in the fit. The size of the HIREFS error bars are statistical; the large scatter in the points and the discrepency with the model give an indication of the large underlying systematic errors.

HRC-I MCP QE			
Energy (eV)	MCP QE	Origin	Error
277	0.39/0.38	FF/XRCF	0.04
290	0.352	Synch	0.04
300	0.326	Synch	0.03
310	0.330	Synch	0.03
320	0.334	Synch	0.03
330	0.329	Synch	0.03
340	0.332	Synch	0.03
350	0.327	Synch	0.03
525	0.30	FF	0.03
851	0.41	FF	0.04
1487	0.34	FF	0.03
2560	0.166	XRCF	0.002
3500	0.126	XRCF	0.002
4510	0.093	XRCF	0.002
4600	0.120	XRCF	0.001
4800	0.117	XRCF	0.001
4900	0.128	XRCF	0.002
4960	0.127	XRCF	0.001
5060	0.149	XRCF	0.002
5130	0.145	XRCF	0.001
5250	0.152	XRCF	0.001
5320	0.152	XRCF	0.001
5480	0.159	XRCF	0.001
5660	0.157	XRCF	0.001
6300	0.156	XRCF	0.002
7000	0.148	XRCF	0.001
8000	0.153	XRCF	0.001
9000	0.168	XRCF	0.002

Table 4: Table of HRC-I QE values. All values except 8000 and 9000 eV were used in the QE interpolation. XRCF errors are purely statistical. FF and Synchrotron errors include 10% systematic contribution.

3.2 Data Products

The final data products including HRC-I QE and HRMA/HRC-I effective area were created by incorporating the transmission of the HRC-I UVIS, HRMA effective area values and the effect of the HRMA cone angles on QE. The effect of the HRMA cone angles on the QE of a HRC-I type MCP is summarized in Figure 7.

The data products are presented in Figures 8 through 12. In addition to these graphical data products, tabular values of QE and EA are attached as appendices to this report. All the data products are also available in tabular form on the HRC calibration website:

`http://hea-www.harvard.edu/HRC/calib/calib.html`

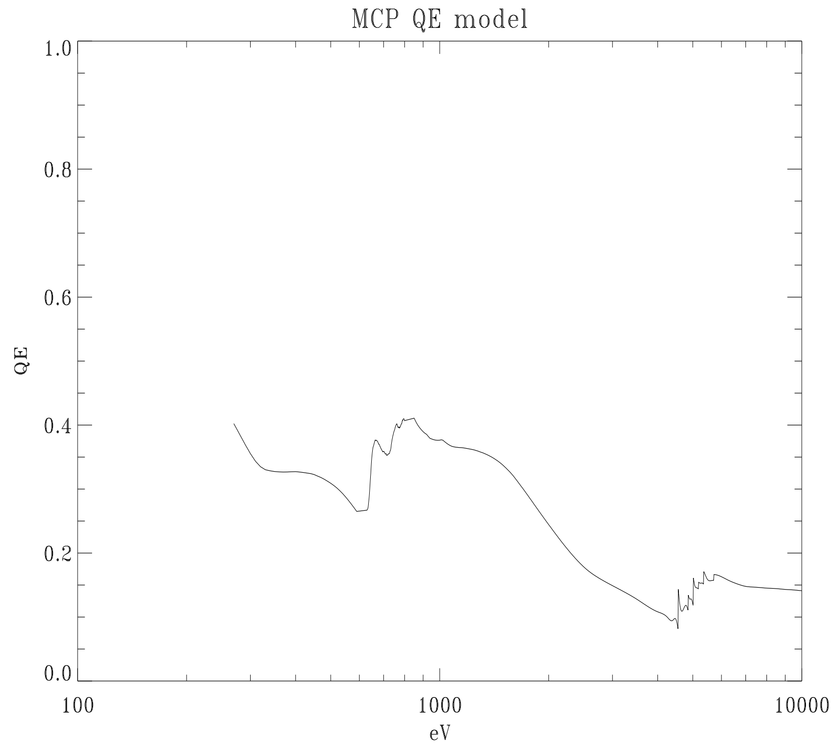

Figure 5: QE of CsI coated HRC-I MCPs. Data from XRCF, Flat field and synchrotron data were incorporated.

3.3 Effective Area

The Effective Area (EA) of the HRC-I in conjunction with the flight HRMA has been calculated. The HRMA model is :

`http://hea-www.harvard.edu/MST/mirror/www/orbit/hrma_ea/hrma_ea_raytrace_scaled_orbit_10arcsec.rdb`

which is the EA within a 10 arc-second diameter and is dated '5-10-99'. The flight HRMA effective area is presented in Figure 10. The flight HRC-I EA is depicted in Figures 11 and 12.

4 Conclusion and Further Work

The QE of the HRCI and the EA of the HRCI in conjunction with the flight HRMA model have been derived using various sources of QE data. In all cases the uncertainty in the final products has been dominated by systematic errors in the original data sets. We estimate that the uncertainty in the FF HRC-I QE measurements to be $\sim$ 10%. The DCM measurements have an estimated systematic error of $\sim$ 7%. The quantitative aggreement between the XRCF and FF QE values at the single 277 eV value give us some confidence that the HRC-I detector changed little due to the post XRCF hardware modifications for $E > 277$ eV. Furthermore this agreement gives us confidence in applying the flat-field to HRMA cone angle corrections to the data.

The disagreement amongst all the measured QE values below C (277eV) has led us to conclude that there is a particular need for more data in this energy regime. It has therefore been decided that no QE values will be quoted for the HRC-I detector below 277eV. A new series of absolute QE value measurements with sample

MCPs will be made at SAO in the next several months. These new laboratory measurements will use flight like MCPs coated at SAO with the same deposition facility and according to the same protocol as was used on the flight MCPs. Using a reflection grating monochromator we will determine absolute QE of these flight representative coated MCPs in the 100 to 1500 eV band. This data will allow us to better determine the HRC-I QE in this energy regime. In addition to laboratory measurements, this energy regime will be investigated during the on-orbit calibration phase of the HRC-I observation program.

5 References

- Henke, B. L.,Knauer, J.P.,Premaratne, K, "The characterization of X-ray photocathodes in the 0.1-10-keV photon energy region". Journal of Applied Physics, vol. 52, Mar. 1981, p. 1509-1520.
- Henke, B. L., Gullikson, E. M., and Davis, J. C., Atom. Data and Nucl. Data Tables, **54**(2), 181, JUL93.
- Juda, M., "A Simple Model for the QE of CsI coated MCPs", SAO Internal Memo, 1997.
- Kenter, A. T. *et al.*, "Performance and Calibration of the AXAF High Resolution Camera I: Imaging Readout", *EUV, X-Ray, and Gamma-Ray Instrumentation for Astronomy VIII*, O. H. W. Siegmund and M. A. Gummin, eds., Proc. SPIE 3114, 1997.
- Kenter, A. T., "HRC QE versus angle of incidence", SAO Internal Memo, September 1998.
- Kraft, R. P., Chappell, J. H., Kenter, A. T., Kobayashi, K., Meehan, G. R., Murray, S. S., Zombeck, M. V., Fraser, G. W., Pearson, J. F., Lees, J. E., Brunton, A. N., and Pearce, S. E., *EUV, X-Ray, and Gamma-Ray Instrumentation for Astronomy*, O. H. W. Siegmund and M. A. Gummin, eds., Proc. SPIE 2808, 1996.
- Kraft, R. P. *et al.*, "Performance and Calibration of the AXAF High Resolution Camera II: Imaging Readout", *EUV, X-Ray, and Gamma-Ray Instrumentation for Astronomy VIII*, O. H. W. Siegmund and M. A. Gummin, eds., Proc. SPIE 3114, 1997.
- Meehan, G. R. *et al.*, "Calibration of the UV/Ion Shields for the AXAF High Resolution Camera", *EUV, X-Ray, and Gamma-Ray Instrumentation for Astronomy VIII*, O. H. W. Siegmund and M. A. Gummin, eds., Proc. SPIE 3114, 1997.
- Murray, S. S. *et al.*, "The AXAF High Resolution Camera (HRC): Calibration ad Recalibration at XRCF and Beyond", *EUV, X-Ray, and Gamma-Ray Instrumentation for Astronomy VIII*, O. H. W. Siegmund and M. A. Gummin, eds., Proc. SPIE 3114, 1997.
- Patnaude, D. *et al.*, "Effective Area of the AXAF High Resolution Camera (HRC)", *EUV, X-Ray, and Gamma-Ray Instrumentation for Astronomy VIII*, O. H. W. Siegmund and M. A. Gummin, eds., Proc. SPIE 3445, 1998.
- Pearce, S. E., Lees, J. E., Pearson, J. F. Fraser, G. W., Brunton, A. N., Flanagan, K. A., Kenter, A., Barbera, M., Dhanak, V., Robinson, A., and Teehan, D., *EUV, X-Ray, and Gamma-Ray Instrumentation for Astronomy VI*, O. H. W. Siegmund and J. V. Vallerga, eds., Proc. SPIE 2518, 1995.
- Rideout, R. A. *et al.*, "Synchrotron Measurements of the Absolute X-ray Quantum Efficiency of CsI-coated Microchannel Plates", *EUV, X-Ray, and Gamma-Ray Instrumentation for Astronomy VIII*, O. H. W. Siegmund and M. A. Gummin, eds., Proc. SPIE 3445, 1998.

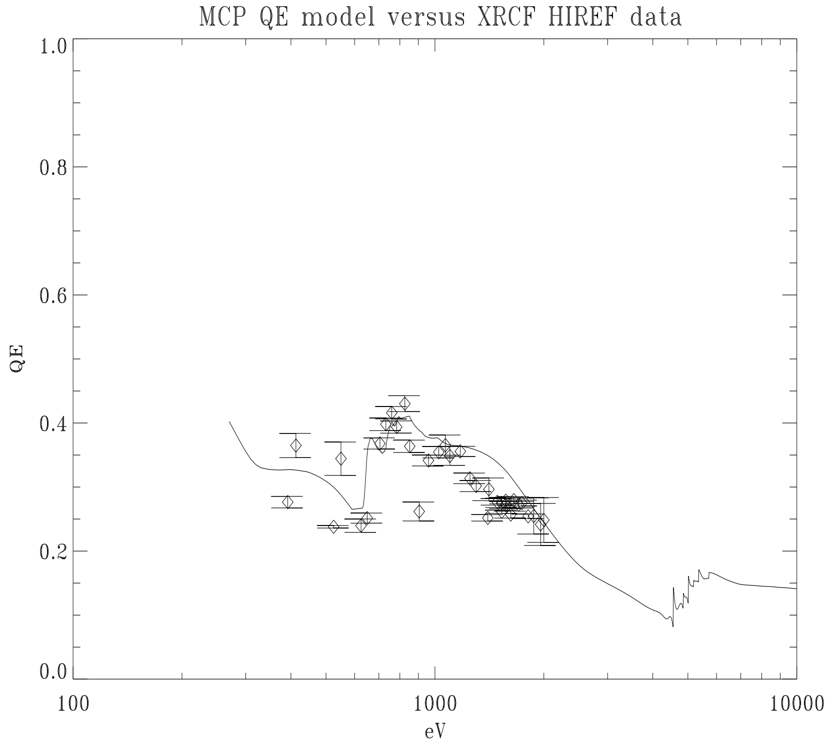

Figure 6: QE of CsI coated HRC-I MCPs versus XRCF HIREFS data that were **not** used in the fit. The HIREFS data had large systematic uncertainty and is only included for qualitative comparison. The HIREFS error bars as shown are purely statistical; the spread of the points give an indication of the underlying large systematic error.

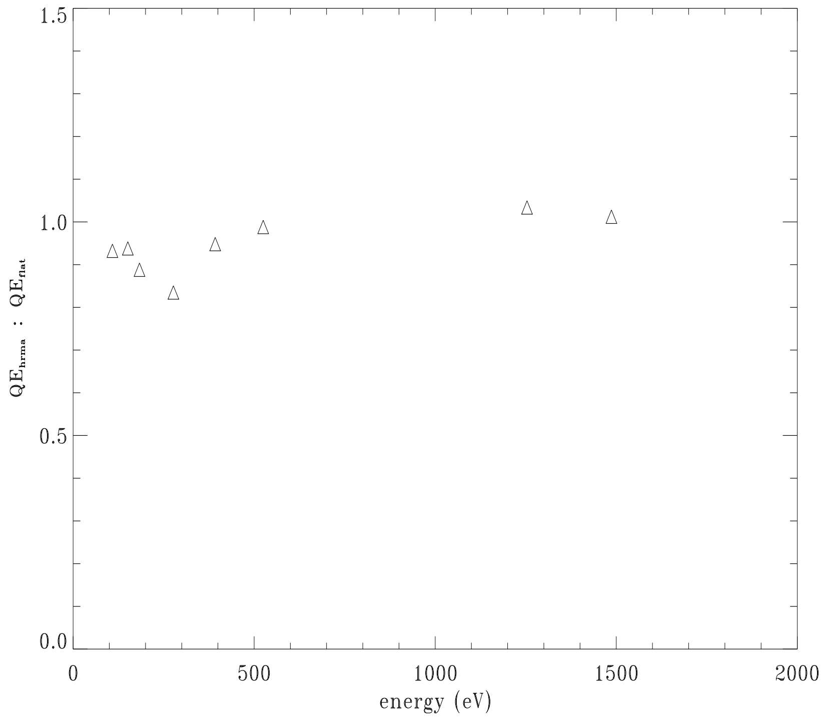

Figure 7: De-rating factors for applying HRC-I flat field data to operation in the converging beam of the HRMA (assuming 4.7° pore bias). Derating factor was interpolated for other energies and was set = 1.0 for higher energies.

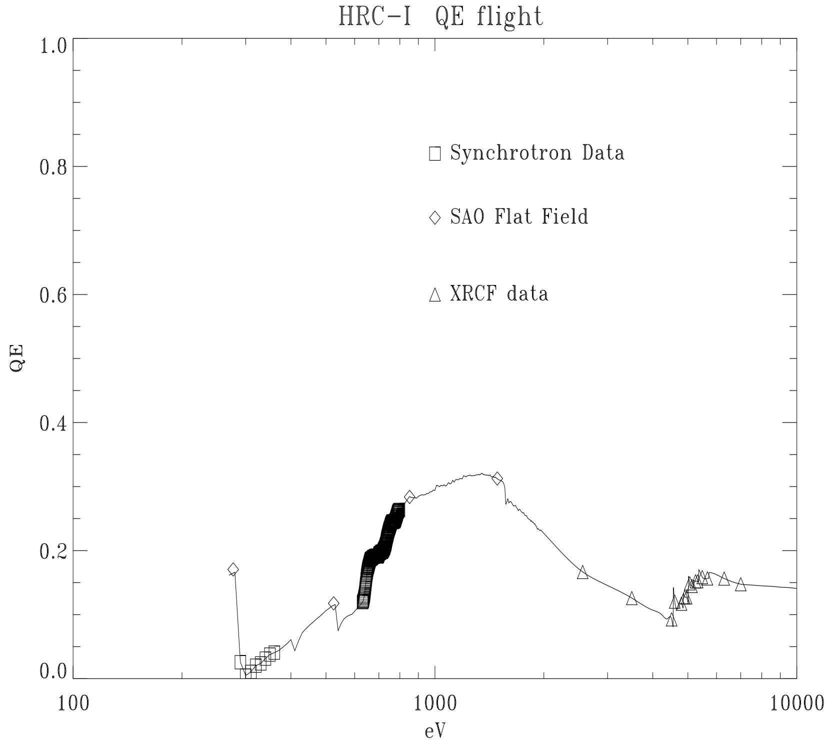

Figure 8: QE of HRC detector incorporating the HRC-I UVIS transmission. The data from XRCF, Flat Field and synchrotron data were incorporated into the HRC QE "model". Flat field and synchrotron data were properly modified to account for HRMA cone angles. The data between $\sim 600-800eV$ are synchrotron values spliced into the final results. The other points were used as input into the electron-range QE interpolation model.

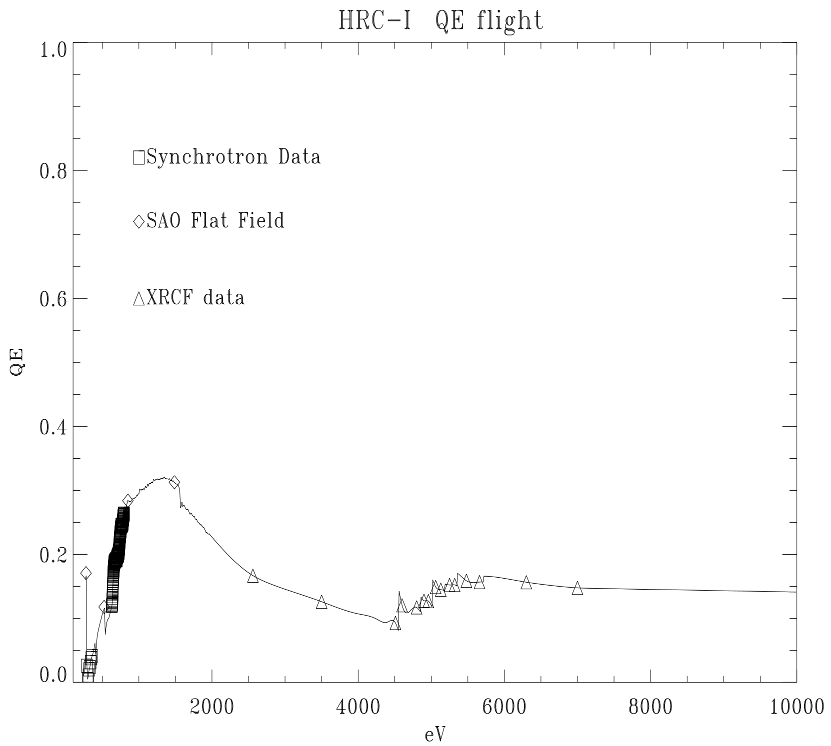

Figure 9: Same data as previous figure except linear energy scale.

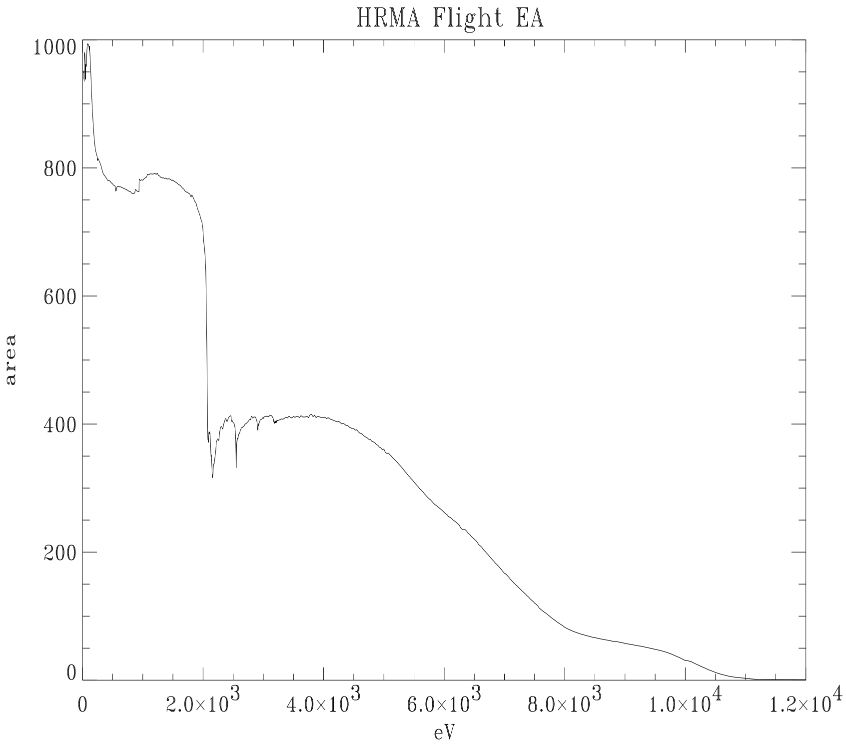

Figure 10: HRMA Effective Area versus energy within 10 arc-sec diameter.

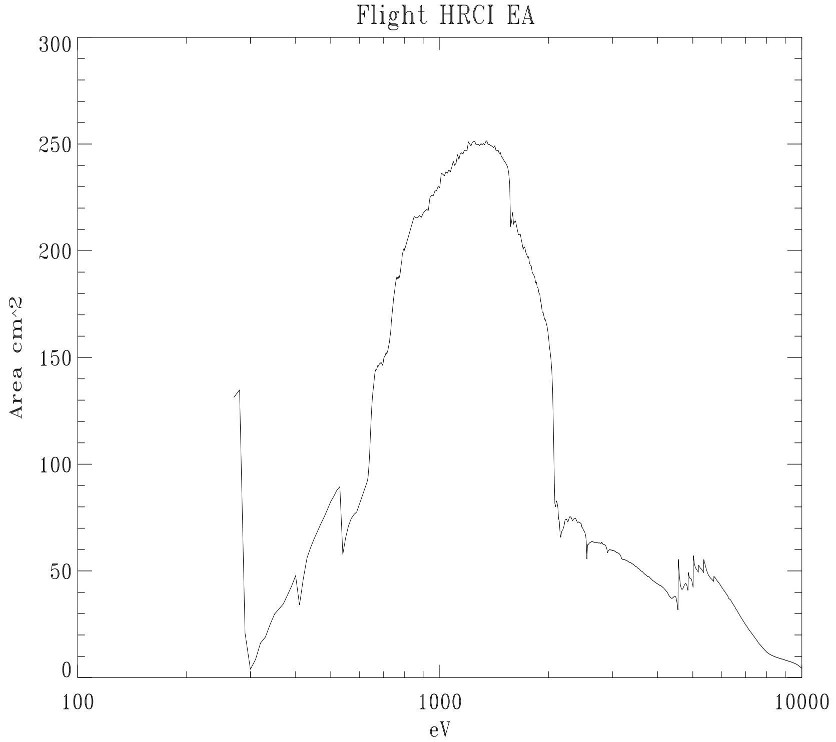

Figure 11: HRC-I/HRMA Effective Area (flight). Log energy scale.

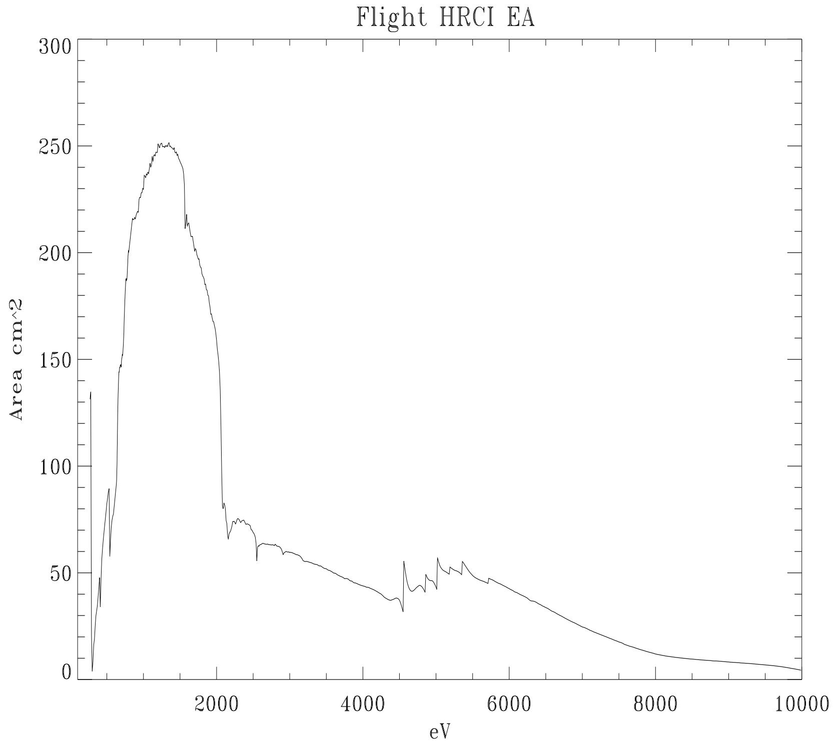

Figure 12: HRC-I/HRMA Effective Area (flight). Linear energy scale.